Surface & Coatings Technology xxx (xxxx) xxx–xxx

Contents lists available at ScienceDirect

Surface & Coatings Technology

journal homepage: www.elsevier.com/locate/surfcoat

Characterizing the micro-impact fatigue behavior of APS and HVOF-sprayed ceramic coatings

J. Kiilakoski[a,*], C. Langlade[b], H. Koivuluoto[a], P. Vuoristo[a]

[a] Laboratory of Materials Science, Tampere University of Technology, P.O. Box 589, FI-33101 Tampere, Finland
[b] Université de Bourgogne Franche Comté, Laboratory ICB-LERMPS UMR CNRS 6303, site UTBM, 90010 Belfort Cedex, France

ARTICLE INFO

Keywords:
Thermal spray
Ceramic coating
Impact test
Fracture
Surface fatigue
Characterization

ABSTRACT

The fatigue life of thermally sprayed Al_2O_3- and Cr_2O_3-based coatings has been studied under low-energy (0.7–5 mJ) impact conditions. A threshold impact energy and amount of repetitions the coatings can endure with said energy before catastrophic failure was obtained. The catastrophic failure was determined to occur when the fracture mode of the coating switched from brittle cone cracking to quasi-plastic radial cracking. The results are examined relative to the microstructural features along with other properties of the coatings - hardness and cavitation resistance. The experiment provided a new approach for a straightforward comparison of the micro-scale impact fatigue life of thermally sprayed coatings unachievable with previous methods.

1. Introduction

Thermal spraying is a common line-of-sight method to produce coatings of a multitude of materials on large surfaces. Often, these coatings are required to exhibit good tribological and chemical resistance. Such applications are found in the process industry e.g. in center press rolls and dewatering elements for paper machines, mechanical seals and process valves. For the demand of such environments demand, coatings deposited from ceramic feedstock are typically the most suitable solution due to their excellent wear properties and chemical inertness. [1,2] However, the main drawback with these coatings is their brittleness [3], which often hinders their usability in applications where impact resistance and ductility are beneficial. Hence, the failure mechanism in ceramic coatings is typically brittle fracture with zero to little plastic deformation. [2] Significant efforts have been put on the improvement of the toughness of ceramic coatings through material processing by incorporating another ceramic phase [4,5], a metallic phase [6] or novel spray processing methods [7–10]. Despite the improvements in fracture toughness, the development of damage during fatigue has a multitude of variables and is not yet fully understood.

As is the case with coatings, the main issue also with traditional ceramics when considering mechanical properties is brittleness. Ceramics cannot relieve stress in their structure, making them sensitive to existing cracks and flaws that dictate the strength of the material. [11] The growth of the crack or flaw under stress is essential to the lifetime of the component: when it reaches a critical size, which is determined by fracture toughness, the component fails. [11–13] The lifetime of the component can be determined by fatiguing tests, such as spherical indentation, where the flaw is intentionally grown until the component fails. The phenomenon of fatiguing under spherical indentation occurs by an initiation and propagation of a tensile-driven “brittle” cone-crack followed by shear-driven “quasi-plastic” radial cracking along with deeply penetrating secondary cone cracks with higher number of repetitions or increasing load. [14–16] To combat the initiation of cracking, Lee et al. [15] have found that in silicon nitride with different microstructures, higher toughness leads to suppression of cone cracking and less strength degradation with increasing indentation loads. They concluded that the quasi-plastic fracture mode is less deleterious to component strength. In another study on the same topic, Kim et al. [16] have studied the transition between the two modes in a fatigue test extensively in soda-lime glass, porcelain and silicon nitride, and observed some degradation in the inert strength of the material during propagation of the cone crack, but severe degradation when radial cracking had commenced. While components in some applications can sustain their ability to function even with cone cracks, radial cracking typically leads to catastrophic failure [16,17]. Therefore, extrapolation of strength values measured from low amount of repetitions was deemed dangerous. Similar deduction was suggested by Quinn et al. [18] for the Vickers indentation experiment, where the increasing load led to declining hardness value until a “brittleness threshold” was reached. They confirmed the results with eight different ceramics. We

* Corresponding author.
E-mail address: jarkko.kiilakoski@tut.fi (J. Kiilakoski).

https://doi.org/10.1016/j.surfcoat.2018.10.097
Received 25 July 2018; Received in revised form 4 October 2018; Accepted 30 October 2018

measured similar results previously on thermally sprayed Cr_2O_3 and TiO_2 –coatings [19], where hardness values lowered with increasing load until the Cr_2O_3 coating catastrophically failed and the TiO_2 coating started to conform to the substrate.

However, limited amount of fatigue testing by indentation has been performed on thermally sprayed ceramic coatings. Ahmed et al. [20] investigated the rolling contact fatigue of thermally sprayed hard metal and ceramic coatings and determined the failure modes as: abrasion, delamination, bulk failure and spalling. From these failure modes, abrasion and bulk failure seem unlikely for ceramic coatings under an indenter due to the fixed site of analysis and the higher susceptibility to damage of the coating in relation to the substrate. Therefore, the probable failure modes are delamination and spalling. These failure modes were defined by the authors as stemming from stress concentrations due to coating defects and subsurface crack initiation and propagation, which would suggest the “quasi-plastic” mode of failure. Vackel et al. [21] investigated the effect of thermal history, microstructure and residual stresses of HVOF-sprayed WC-CoCr coatings on a component lifetime in a bending fatigue test. They determined that higher hardness and compressive stresses were advantageous to the fatigue life of the system. In a similar test, Ibrahim et al. [22] confirmed that compressive residual stresses and a higher elastic modulus are desired for fatigue life improvement. Due to these properties, they found an improvement of HVOF-sprayed over APS-sprayed TiO_2.

Impact fatigue of coatings is, however, quite different from the mentioned circumstances since the Hertzian contact is highly localized and mainly compressive under the indent with some additional shear. [23] On the topic of hertzian impacts, Musalek et al. [24] used spherical indentation to observe changes in the microstructure of an alumina coating sprayed with a water-stabilized plasma system after a single indentation. They discovered cracking, closing of existing cracks, debonding and sliding on the splat interfaces, which would suggest a “quasi-plastic” behavior as previously defined. Other considerations for coatings are the lower initiation loads for cone cracks for thin coatings (thickness smaller than the diameter of the indenting sphere) [17] and that segregate phases on grain boundaries lead to high compressive stresses on the boundaries, which in turn emphasizes “brittle” fracture mode [25]. The consequence of these considerations is that the lack of compressive stresses at the splat boundaries lead to a preference to shearing under indentation, and the low thickness of the coating can further lower the initiation threshold of conical cracking. Therefore, it is logical to turn attention towards measuring the onset of the quasi-plastic regime, when catastrophic failure occurs.

To study this phenomenon, one suitable measure would be impact fatigue resistance under controlled conditions and a small enough scale. Such equipment has been utilized to study the phase-transformation in metals [26,27] and damage behavior of thin hard coatings [28]. In these studies the precisely controllable impact energy and location has allowed for meticulous examination of the impacts leading to models of critical stress levels for the materials as well as studying of the microstructural changes during a fatiguing at a controlled time. The micro-impact fatigue experiment in question would potentially give a new method of studying the development of fracturing in thermally sprayed ceramic coatings as well, where it has not yet been applied.

The objective of this study is to find the impact energy limits where selected plasma- and HVOF-sprayed ceramic coatings have their transformation from brittle to quasi-plastic cracking leading to catastrophic failure. This is achieved by exploring their mechanical response when subjected to a repeated number of impacts with different loads, followed by different number of impacts with a constant load. These results are then compared with other measured mechanical properties of the coatings.

2. Experimental methods

Thermally sprayed Al_2O_3- and Cr_2O_3-based ceramic coatings on 1.0841 steel substrates were examined in this study. The coatings were sprayed with two methods: atmospheric plasma-spray (APS, F4 torch, Oerlikon Metco AG, Winterthur, Switzerland) and high-velocity oxy-fuel spray (HVOF, TopGun, GTV Gmbh, Luckenbach, Germany) from feedstock powders provided by three different manufacturers (H.C. Starck GmbH, Munich, Germany; Ceram GmbH, Albbruck-Birndorf, Germany and Millidyne Oy, Tampere, Finland). The target coating thickness was 250–300 µm, which was approximated by measuring with a Surfix easy-coating thickness gauge (Phynix GmbH & Co. KG, Neuss, Germany). The deposition parameters have been optimized in previous studies with the aim of achieving a dense microstructure and high hardness for wear applications. The information on the powders and the coating deposition parameters can be found in Tables 1 & 2.

Table 1
Processing parameters of the APS-coatings.

Sample name	APS-Al_2O_3	APS-Al_2O_3-40ZrO_2	APS-Cr_2O_3
Powder manufacturer	H.C. Starck	Ceram	H.C. Starck
Material chemical composition [wt%]	Al_2O_3	Al_2O_3-40ZrO_2	Cr_2O_3
Powder manufacturing method	Fused & crushed (F&C)		
Powder size distribution [µm]	−45 + 22	−45 + 20	−45 + 22
Ar [slpm]	41	41	38
H_2 [slpm]	14	13	13
Current [A]	610	610	630
Voltage [V]	74	70	73
Powder feed rate [g/min]	39	45	51
Standoff distance [mm]	110	140	110
Relative surface speed [m/min]	96	87	107
Offset [mm/pass]	6	7	6
Passes [number]	60	36	74
Coating thickness [µm]	~300	~300	~421

The coating cross-sections were prepared by grinding up to P1200 grit paper and consequently polishing up to a ¼-µm diamond slurry. The coating hardnesses were determined from ten indentations on the cross-section using a Vickers hardness tester (MMT-X7, Matsuzawa, Akita, Japan) with a load of 300 gf ($HV_{0.3}$) and the coating microstructures were characterized with a scanning electron microscope (XL30, FEI Company/Thermo Fisher Scientific Inc., Hillsboro, OR, United States).

The micro-impact fatigue experiments were performed with an in-house –made apparatus at Université de Technologie de Belfort-Montbéliard (Sevenans, France) of which a schematic is presented in Fig. 1. The input parameters are excitation time of the electromagnet that accelerates the indenter in milliseconds and the amount of repetitions. The distance between the sample and the indenter was kept constant at 0.7 mm and the velocity of the indenter was measured, as well as the load induced on the sample. The velocity and load measurements were performed for the first and last five repetitions, as well as once in the middle of the set for five repetitions. In the first set of experiments, a 2 mm diameter ZrO_2-ball indenter was used with repetitions of 1000 and the excitation time was increased from 0.7 ms to 1.1 ms with 0.1 ms increments (corresponding roughly to loads of 100 to 600 N or impact energies of 0.7 to 5 mJ). In the second set, fixed excitation times were used for each sample based on their perceived damage while varying the repetitions from 100 to 1000 in order to find the energy/repetition amount the sample can endure. For further examination, the impact energy values were chosen over load values due to the effect of substrate thickness and properties, such as acoustic impedance, on the measured load. This enables simpler comparison between coatings on various substrates without additional variables in the future. In all fatigue tests, the frequency of the impacts was 10 Hz. More details of the test can be found e.g. in [26,28,29]. Before the experiments, the coating surfaces were ground with P600 and P1200 SiC-papers and polished with a 3 µm diamond slurry to achieve as similar a surface topography as possible. The coating thicknesses were

Table 2
Processing parameters of the HVOF-coatings.

Sample name	HVOF-Al_2O_3	HVOF-Al_2O_3-40ZrO_2	HVOF-Cr_2O_3	HVOF-Cr_2O_3-3TiO_2	HVOF-Cr_2O_3-5TiO_2
Powder manufacturer	H.C. Starck	Ceram	Saint-Gobain	Millidyne	Millidyne
Material chemical composition [wt%]	Al_2O_3	Al_2O_3-40ZrO_2	Cr_2O_3	Cr_2O_3-3TiO_2	Cr_2O_3-5TiO_2
Powder manufacturing method	Fused & crushed			Agglomerated & sintered	
Powder size distribution [μm]	−20 + 5	−25 + 5	−15 + 5	−30 + 10	−25 + 8
C_2H_4 [slpm]	93	90	137	127	130
O_2 [slpm]	270	257	288	275	308
O_2/C_2H_4-ratio	2.9	2.9	2.1	2.2	2.37
Powder feed rate [g/min]	40	30	20	25	15
Standoff distance [mm]	150	150	150	150	170
Relative surface speed [m/min]	179	179	179	179	80
Offset [mm/pass]	3	3	3	3	3
Passes [number]	24	36	60	60	60
Coating thickness [μm]	~250	~330	~200	~220	~240

measured to ensure no more than 50 μm of coating was removed during the preparation. The impact craters were examined with an optical microscope as well as an optical profilometer (Infinitefocus G5, Alicona Imaging GmbH, Austria) to obtain their volume loss after the experiment.

Additionally, the cavitation erosion resistance of the coatings was measured to compare another mechanical property with the micro-impact fatigue test. The cavitation erosion was performed with an ultrasonic transducer (VCX-750, Sonics & Materials, Newtown, USA), according to the ASTM G32-10 standard for indirect cavitation erosion. The vibration tip was an alloy of Ti-6Al-4V. The sample surfaces were ground flat and polished with a polishing cloth and diamond suspension (3 μm). Samples were cleaned in an ultrasonic bath with ethanol and weighed after drying. Samples were attached on a stationary sample holder and the head of the ultrasonic transducer was placed at a distance of 0.5 mm. Samples were weighed after 15, 30, 60 and 90 min. The cavitation resistance of the coatings was calculated as the reciprocal of the mean-depth of erosion per hour, which in turn is derived from the theoretical volume loss (presuming a fully dense coating) and the area of the vibrating tip.

3. Results & discussion

The micrographs of the cross-sections of the coatings are presented in Fig. 2. All coatings were of good quality with a high melting degree and some intrinsic porosity. The thicknesses were roughly 300 μm for all coatings. The APS-coatings exhibited larger micro features due to the larger feedstock particle size whereas the structure of the HVOF-samples was finer throughout. The APS Al_2O_3 and Cr_2O_3-coatings are representative of typical APS-coatings by having clear borders between lamellas as well as intralamellar cracking. In HVOF-sprayed Cr_2O_3-3TiO_2 and Cr_2O_3-5TiO_2, metallic lamellae from particles reduced during spraying are visible as lighter, homogeneous splats. When comparing the Al_2O_3-40ZrO_2-coatings, the melting degree of the lighter Zr-rich phase is clearly higher in the APS- than the HVOF-sample along with more of the light grey mixed Al_2O_3-ZrO_2-phase.

3.1. Micro-impact fatigue with constant repetitions and varying impact energies

The samples were subdued to 1000 impacts with differing excitation times of the impactor, leading to differing impact energies. Optical micrographs of the impact sites on the samples after the first experiment are presented in Figs. 3 and 4. All samples were relatively unaffected by 1000 impacts of the shortest excitation time of 0.7 ms (ca. 1.3 J energy input). From some samples, even distinguishing the impact site proved impossible, indicating the absence of cone cracks. These appeared with 0.8 ms (ca. 2 J) for the rest of the coatings, but the first differences were found with 0.9 ms (ca. 3 J) when the HVOF-Cr_2O_3-sample shattered indicating heavy radial cracking. This was followed by similar catastrophic failure of the HVOF-Cr_2O_3-3TiO_2-sample at 1.0 ms (ca. 4 J). With this impact energy, also all of the other coatings exhibited prominent rings of cracks around the craters that could be interpreted as failure, albeit vastly milder than with the two coatings mentioned above. The harshest conditions (1.1 ms/ca. 4.5–5 J) produced similar craters as the previous ones, only slightly larger. Altogether the crater development is very similar to what has been reported for traditional bulk ceramics [16], where ring cracks appeared already after one impact and radial cracking commenced only after a large amount of repetitions.

The test gives a seemingly large variation of impact energies with the same excitation time. However, since the energy was only calculated form 15 repetitions out of 1000 in each case, it is believed that over the whole test the energies are averaged to essentially similar values for each coating. For the concurrently ran load measurements the variation was significantly smaller but as outlined in section 2, utilizing the load values are not desirable due to differences in substrate properties. From the optical micrographs the following conclusions can

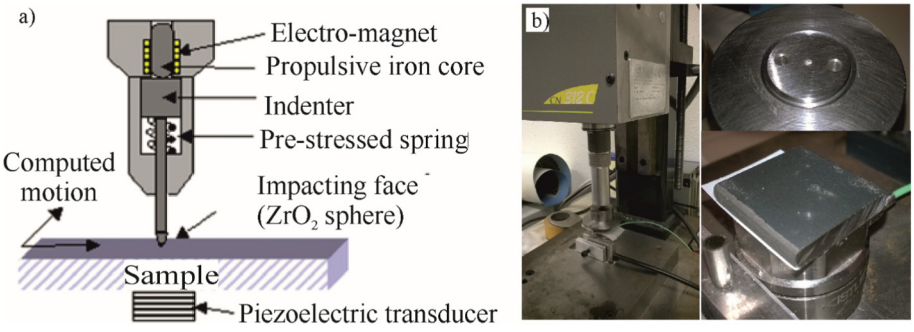

Fig. 1. a) A schematic presentation of the micro-impact fatigue test apparatus. Modified from [13]. b) Images of the test setup, the impacting ball and the sample attached to the load cell.

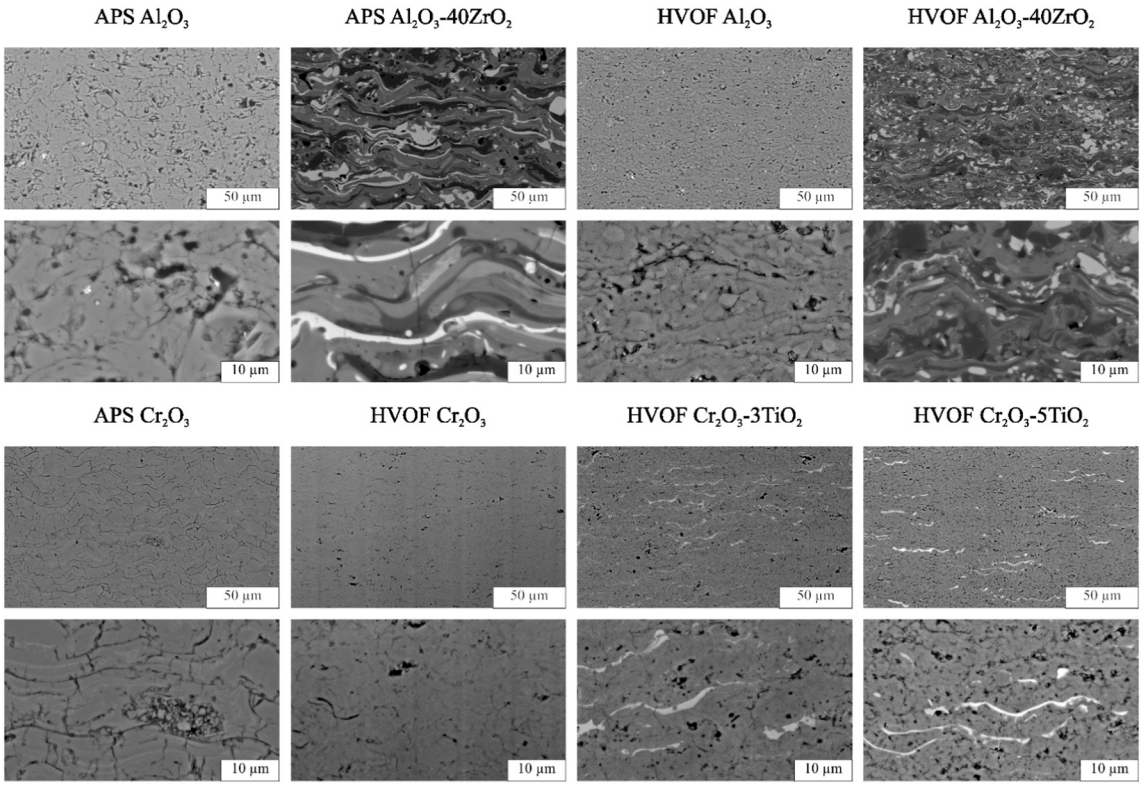

Fig. 2. Cross-sections of the coatings tested in the study. SEM (BSE)-images.

be drawn: 1) The Cr_2O_3-based HVOF coatings are very resistant to impact fatigue on small loads, in fact in many cases no cone cracking appeared on the coatings. 2) When the impacting energy reaches a critical level the HVOF Cr_2O_3 coating fails catastrophically. This is likely due to the high internal stresses stemming from the considerably higher deposition temperature [30]. However, adding TiO_2 increases the resistance of the coating to this behavior by lowering the melting point of the ceramic composite mixture. 3) Plasma-sprayed coatings and HVOF-sprayed Al_2O_3-based coatings exhibit a more gradual propagation of cone cracking, i.e. development of damage, as a function of impact energy. This is possibly due to lower internal stresses stemming from lower heat loads to the substrate. 4) It is very challenging to determine the exact point where the radial cracking and therefore failure commence visually, since a visible cone crack crater already exist in

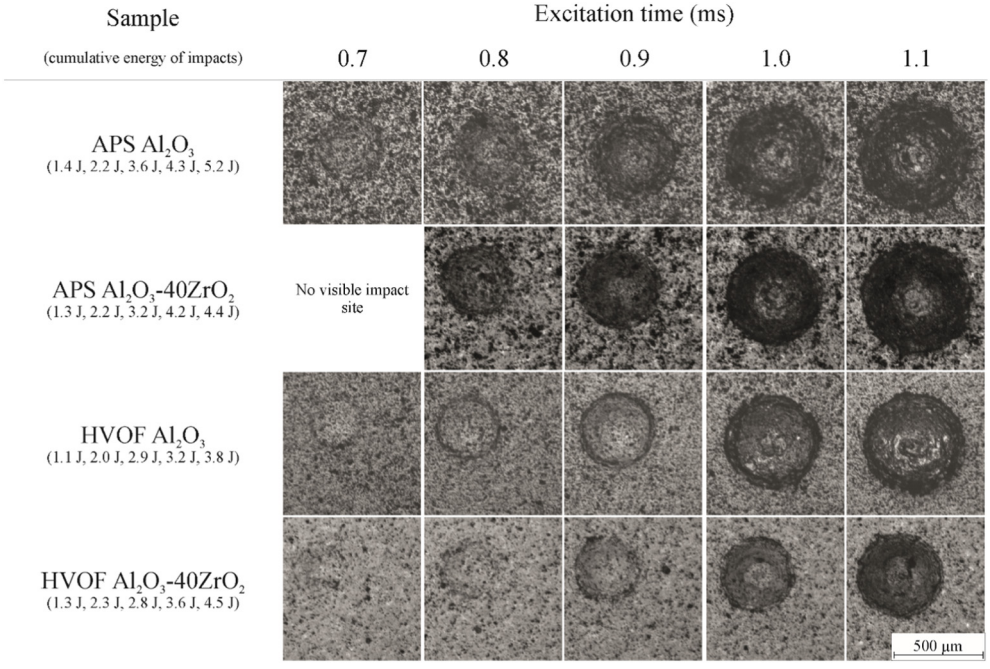

Fig. 3. Optical micrographs of the impact craters of the Al_2O_3-based coatings after the micro-impact fatigue experiment with fixed amount of repetitions. The scale bar is the same for all images.

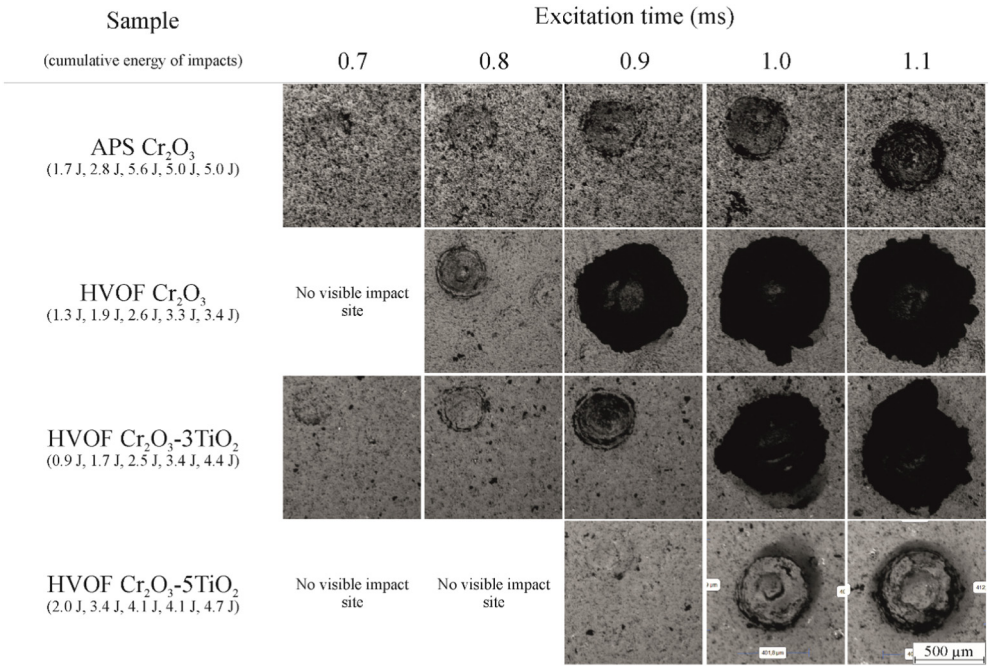

Fig. 4. Optical micrographs of the impact craters of the Cr_2O_3-based coatings after the micro-impact fatigue experiment with fixed amount of repetitions. The scale bar is the same for all images.

most cases even at small loads and its propagation and the appearance of radial cracking is very gradual.

The visual method of observing the failure is very subjective due to the difficulty of determining the exact point of failure and, therefore, efforts were put forth to find a way to determine failure numerically. For this reason, the volumes of the craters were measured and are presented in Table 3. Clearly, there are large differences in crater volumes between the coatings and the enlargement of the crater can be determined as a function of impact energy. The outlier of the group is HVOF Cr_2O_3-5TiO_2 where the crater was smaller with the 1.1 ms impact than 1.0 ms, seen as a negative change in normalized volume in Table 3. This is deemed to be a result of the debris from the crater remaining somewhat attached to the coating (as seen in Fig. 4) distorting the measurement. Despite the seemingly gradual increase in the volume of the crater in the optical micrographs, there seems to exist one greater increase in the measured volume with each coating. Hence, the volume values were normalized to the largest measured crater volume (V_{max}) of each coating, and their increase/decrease was evaluated as percentage points [pp] with the increase in excitation time, Eq. (1).

$$\Delta V\,[pp] = \frac{V_n - V_{n-1}}{V_{max}} \times 100 \tag{1}$$

Comparing the change in normalized volume and the optical micrographs it was observed than typically an increase in normalized volume of 15 pp. of more coincided with also the visual point of catastrophic failure in those cases where visual determination was possible. This is of course an arbitrary value, but seems to correlate well in all cases and will be useful when estimating the performance of the coating whose failure method was more gradual and difficult to distinguish visually. The idea is analogous to the sudden drop in inert strength as measured for bulk ceramics as a function of load cycles [16,25]. The crater volumes and the relative changes are presented in Fig. 5.

Table 3
Crater volumes and incremental volume changes to the previous crater. The points of failure are in bold.

Sample	Attribute	Excitation time [ms]				
		0.7	0.8	0.9	1	1.1
APS-Al_2O_3	Crater volume [$\mu m^3 \times 10^{-3}$]	120	295	616	1179	2149
	Volume change [pp]	–	8.1	14.9	**26.2**	45.1
APS-Al_2O_3-40ZrO_2	Crater volume [$\mu m^3 \times 10^{-3}$]	37	229	518	1432	2629
	Volume change [pp]	–	7.3	11.0	**34.8**	45.5
HVOF-Al_2O_3	Crater volume [$\mu m^3 \times 10^{-3}$]	19	71	189	558	953
	Volume change [pp]	–	5.5	12.4	38.7	41.4
HVOF-Al_2O_3-40ZrO_2	Crater volume [$\mu m^3 \times 10^{-3}$]	18	54	121	319	769
	Volume change [pp]	–	−4.7	8.7	**25.7**	58.6
APS-Cr_2O_3	Crater volume [$\mu m^3 \times 10^{-3}$]	50	106	207	403	764
	Volume change [pp]	–	7.4	13.2	**25.7**	47.3
HVOF-Cr_2O_3	Crater volume [$\mu m^3 \times 10^{-3}$]	49	83	12,730	17,284	24,035
	Volume change [pp]	–	0.1	**52.6**	18.9	28.1
HVOF-Cr_2O_3-3TiO_2	Crater volume [$\mu m^3 \times 10^{-3}$]	8	40	266	8503	16,069
	Volume change [pp]	–	0.2	1.4	**51.3**	47.1
HVOF-Cr_2O_3-5TiO_2	Crater volume [$\mu m^3 \times 10^{-3}$]	–	–	79	95	76
	Volume change [pp]	–	–	–	**17.1**	−20.2

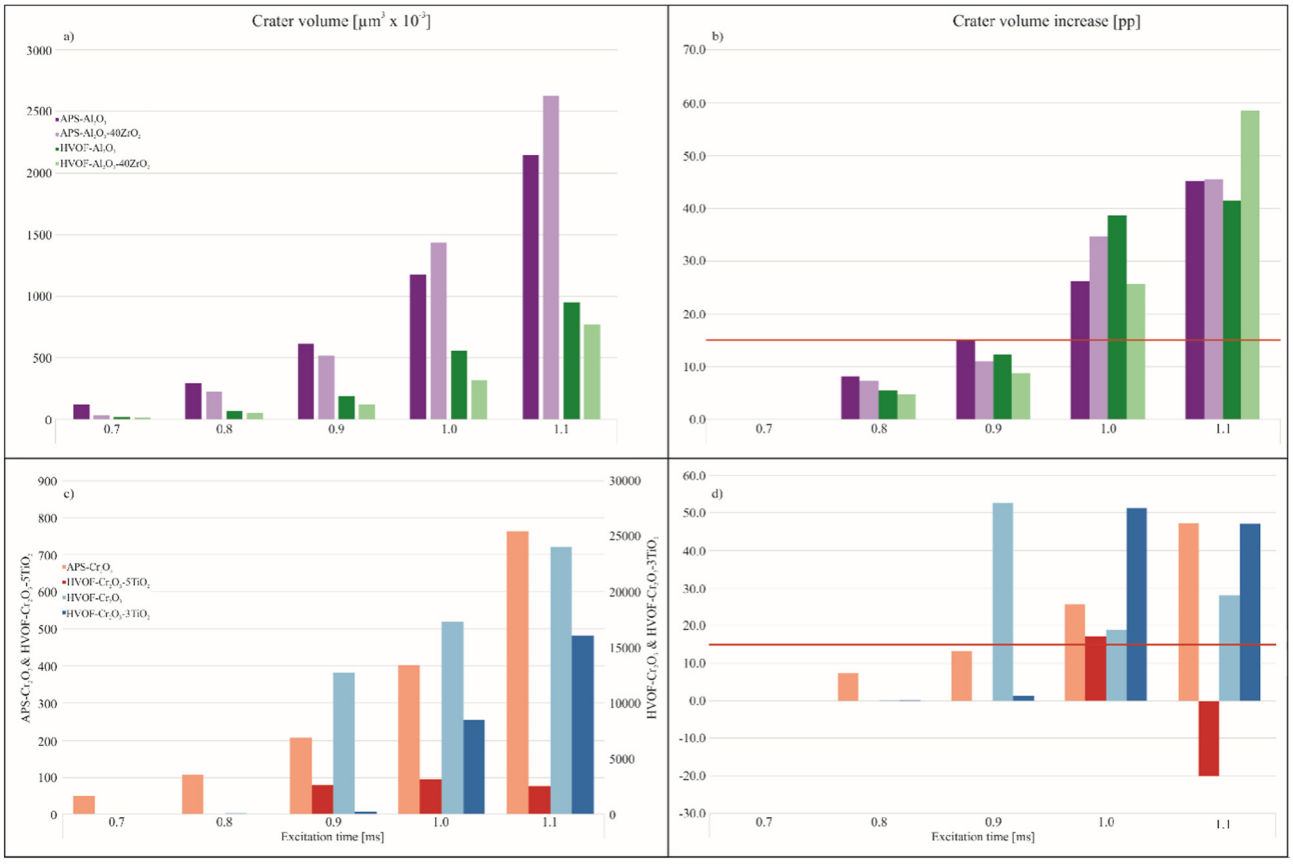

Fig. 5. Graphs of the measured crater volumes for a) Al_2O_3-based samples, b) Cr_2O_3-based samples and the changes in normalized crater volume for c) Al_2O_3-based samples d) Cr_2O_3-based samples. Constant repetitions, variable excitation time.

3.2. Micro-impact fatigue with constant impact energy and varying repetitions

The second set of experiments was conducted with the excitation time determined in the previous step to lead to failure for each coating separately, while the repetitions were increased as follows: 100, 200, 400, 600, and 800. Note that this excitation time was chosen based on the visual inspection of the optical images only, before measurement of the crater volumes. Hence, the excitation times are higher with samples APS Cr_2O_3, HVOF Al_2O_3, HVOF Al_2O_3-40ZrO_2 and HVOF Cr_2O_3-5TiO_2 than the final ones determined from the crater volumes. Since from the micrographs there was some uncertainty which excitation time lead to failure the higher one was chosen to ensure catastrophic failure is achieved during the 1000 impacts. Optical micrographs of the samples after the second experiment are presented in Figs. 6 and 7.

All samples demonstrate visual markings of cone cracking already with 100 repetitions with the chosen excitation times. HVOF-samples Cr_2O_3, Cr_2O_3-3TiO_2 and Cr_2O_3-5TiO_2 exhibited a clear point of failure at 400, 800 and 400 repetitions, respectively. The Cr_2O_3-sample endured by far the highest temperatures during spraying, probably leading to the most compressive stress profile in comparison, leading to it being the first to fail. The Cr_2O_3-3TiO_2 and Cr_2O_3-5TiO_2 were more similar, due to the different impact energies utilized, but likely the 5TiO_2-alloyed sample failed first also due to higher compressive stresses due to a higher (stoichiometric) flame temperature. For the Al_2O_3-based samples and APS Cr_2O_3, the damage development between increasing repetitions was very gradual and the point of failure was again difficult to distinguish. Therefore, the same approach as the first set was utilized and the volume losses and changes in normalized volume loss were measured and are presented in Table 4. The last values with 1000 repetitions are from Table 3, highlighting the variation between the tests in some coatings. Unlike with the first experiment, here negative values of volume change were recorded in multiple occasions with increasing repetitions. This can arise from the relatively small difference in total impact energy, and variation from the difference with the sample distance from the impactor due to unevenness of the samples. The crater volumes and changes in volume are visualized in Fig. 8.

Since different excitation times were used for the samples, a comparison of cumulative impact energies is a viable way to compare the ability of the samples to resist micro-impact fatigue. This is calculated by multiplying the incoming impact energy by the amount of repetitions that lead to failure. This way, both the used excitation time and repetition amount are accounted for in the comparison. Since the durability can only be determined to the accuracy of 100 or 200 repetitions, the range of energies between the last stage of no failure and after failure is given. The samples are presented in order of least resistance to micro-impact fatigue based on these values in Fig. 9.

From the second experimental set, the following conclusions can be drawn; 1) It seems to be irrelevant whether Al_2O_3 or Cr_2O_3 is the base constituent of the coating material. 2) The spray parameter requirements, such as flame temperature, placed by the material have a large effect on the microstructure through residual stresses generated by the thermal history of the sample [30] and hence the fatigue life of the coating. Typically compressive stresses in the coatings are advantageous to tensile fatigue tests [21,22,31], but when the stresses area excessive they become deleterious. 3) Alloying phases can change the behavior greatly: addition of TiO_2 into Cr_2O_3 and ZrO_2 into Al_2O_3 increases fatigue resistance. This effect is either due to their lower hardness [11,32] that are more malleable or to lowering the melting point of the materials and therefore assisting the deposition.

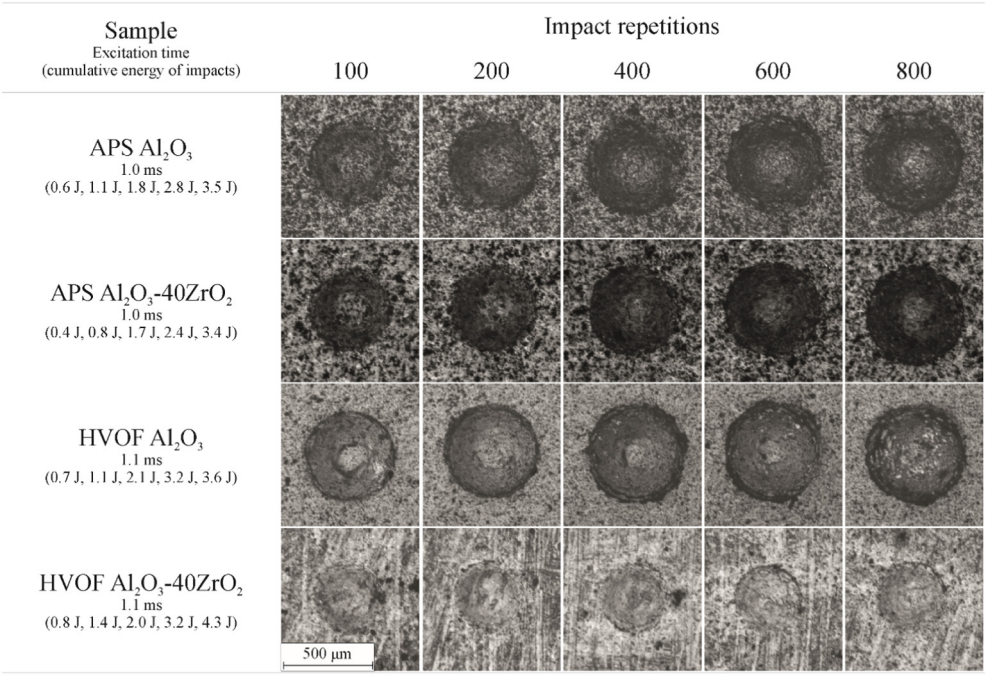

Fig. 6. Optical micrographs of the impact craters of the Al_2O_3-based coatings after the micro-impact fatigue experiment with fixed excitation time and varying repetitions.

3.3. Hardness and cavitation erosion resistance

To investigate the significance of the results further, the hardness values and cavitation erosion resistance values of the coatings are compared and presented in Fig. 10. Vickers hardness value is typically indicative of the crack propagation resistance and structural integrity of the coating [22] in a scale of some tens of micrometers when indented from the cross-section, while cavitation erosion resistance is thought to be a good measure of the coating cohesion and resistance to repeated impacts in a scale of about 10 µm [33]. Generally, HVOF-sprayed samples have a higher hardness and cavitation erosion resistance. The reason for the difference in hardness lies in a finer microstructure, lower porosity [34] and ability to deflect the propagating crack due to unmelted/nanostructured zones [35]. The difference in cavitation erosion resistance stems from the fine microstructure being able to deflect cavitating bubbles better [33].

The order of the samples is kept the same to underline that there is no clear connection between either hardness or cavitation resistance and the results of the micro-impact fatigue experiment. The Cr_2O_3-based coatings are harder (1150–1600 $HV_{0.3}$) than Al_2O_3-based

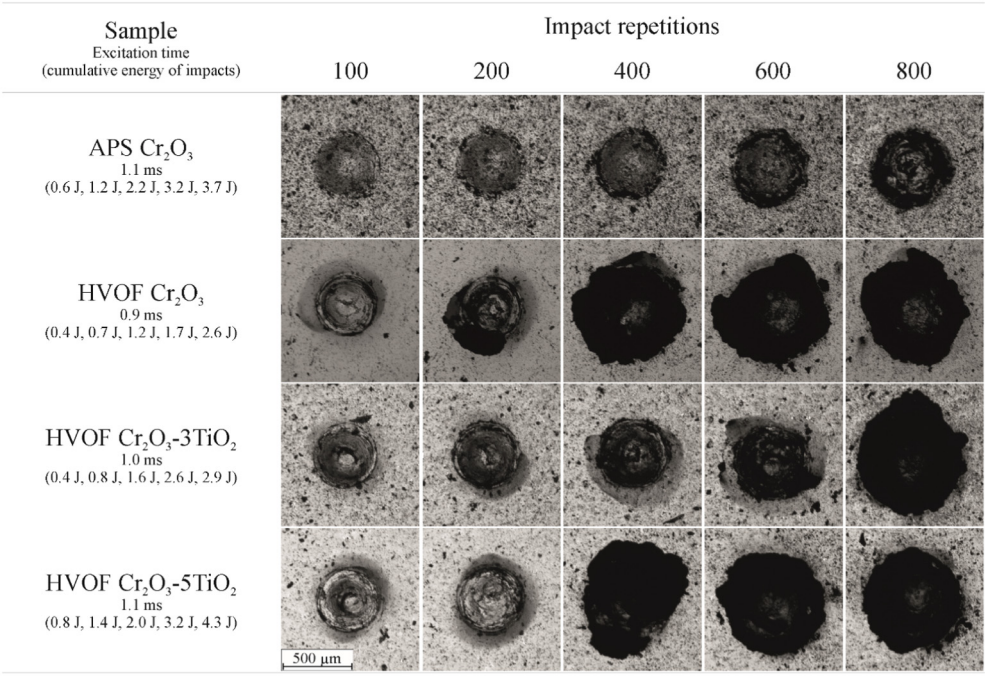

Fig. 7. Optical micrographs of the impact craters of the Cr_2O_3-based coatings after the micro-impact fatigue experiment with fixed excitation time and varying repetitions.

Table 4
Crater volumes and incremental volume changes to the previous crater. The points of failure are in bold.

Sample	Attribute	Repetitions					
		100	200	400	600	800	1000
APS-Al_2O_3	Crater volume [$\mu m^3 \times 10^{-3}$]	526	755	978	1096	1297	1179
	Volume change [pp]	–	**17.6**	17.2	9.1	15.5	−9.1
APS-Al_2O_3-40ZrO_2	Crater volume [$\mu m^3 \times 10^{-3}$]	603	684	881	897	1331	1432
	Volume change [pp]	–	5.7	13.8	1.1	**30.3**	7.1
HVOF-Al_2O_3	Crater volume [$\mu m^3 \times 10^{-3}$]	586	629	784	725	758	953
	Volume change [pp]	–	4.5	**16.3**	−6.2	3.5	20.4
HVOF-Al_2O_3-40ZrO_2	Crater volume [$\mu m^3 \times 10^{-3}$]	199	175	146	192	225	769
	Volume change [pp]	–	−3.1	−3.8	6.0	4.4	**70.7**
APS-Cr_2O_3	Crater volume [$\mu m^3 \times 10^{-3}$]	506	615	678	889	882	764
	Volume change [pp]	–	12.2	7.2	**23.7**	−0.8	−13.2
HVOF-Cr_2O_3	Crater volume [$\mu m^3 \times 10^{-3}$]	336	1697	10,183	10,591	9430	12,730
	Volume change [pp]	–	10.7	**66.7**	3.2	−9.1	25.9
HVOF-Cr_2O_3-3TiO_2	Crater volume [$\mu m^3 \times 10^{-3}$]	650	850	1148	1751	15,823	8503
	Volume change [pp]	–	1.3	1.9	3.8	**88.9**	−46.3
HVOF-Cr_2O_3-5TiO_2	Crater volume [$\mu m^3 \times 10^{-3}$]	288	139	9729	10,209	8548	76
	Volume change [pp]	–	−1.5	**93.9**	4.7	−16.3	−83.0

coatings (800–1050 $HV_{0.3}$) as is typically the case [3,36]. Within the same material, utilizing HVOF-spray instead of APS provided higher hardnesses for the reasons outlined in the previous paragraph. Alloying led to no significant change in hardness for the materials. Based on hardness values, no connection with impact-fatigue behavior exists. In fact, the three hardest coatings, Cr_2O_3, Cr_2O_3-5TiO_2 and Cr_2O_3-3TiO_2 are quite different in their micro-impact fatigue resistance.

Cavitation erosion resistance is more of a function of the spray method, and consequently the APS-coatings perform poorly in this experiment. This is likely due to the larger globular pores [34] that readily act as bubble nucleation sites where erosion initiates rapidly [33]. The Cr_2O_3-based coatings are more resistant to cavitation than Al_2O_3-coatings, but alloying with ZrO_2 improves the performance of Al_2O_3-coatings to equal or higher levels. The finest feedstock size, −15 + 5 µm, of the HVOF Cr_2O_3-coating leads to the finest microstructure and again to the highest cavitation erosion resistance. The connection to hardness exists in that microhardness is more influenced by the material property and cavitation resistance is a combination of material choice with the scale and quality of the microstructure. As presented in Fig. 10, neither of these properties correlate with the repeating micro-impact fatigue

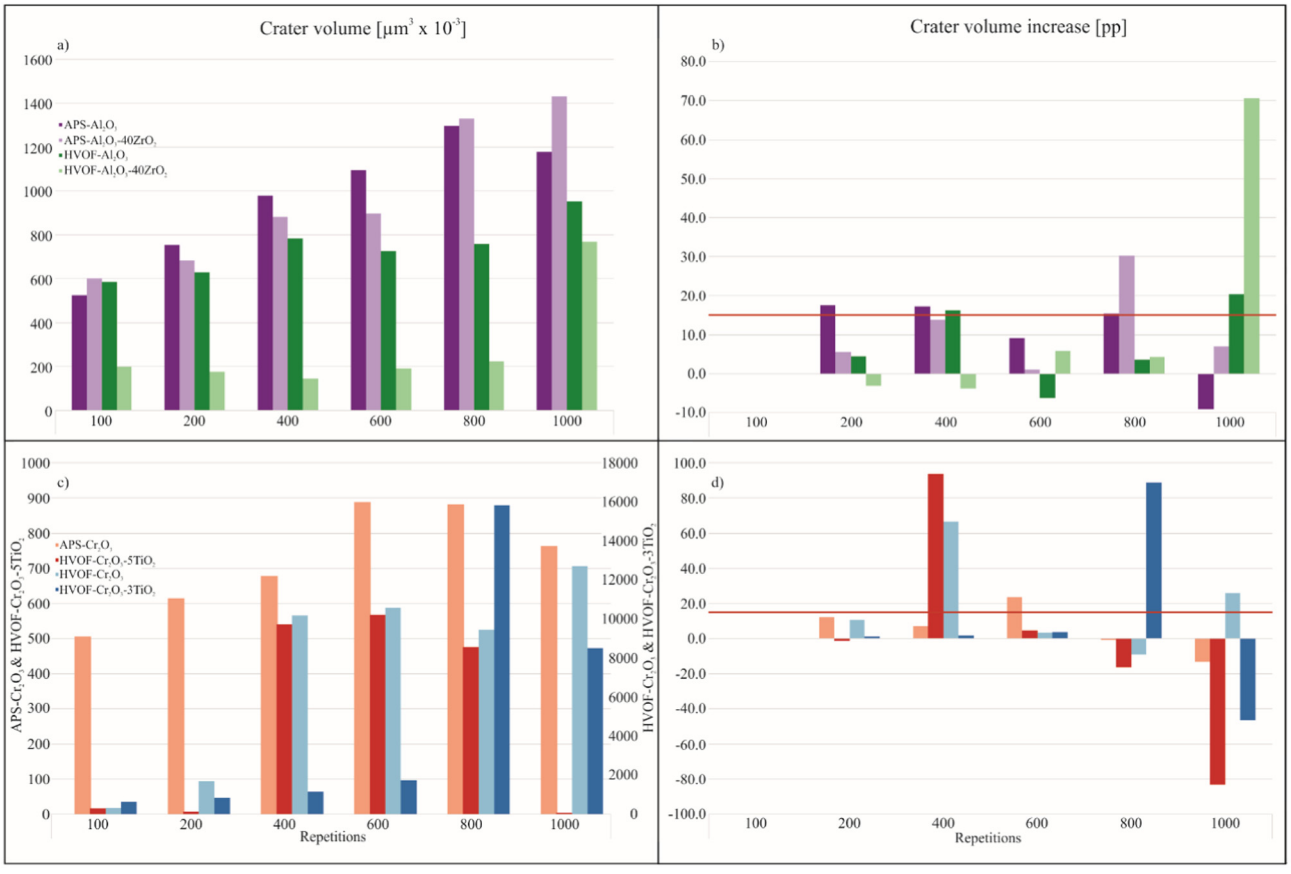

Fig. 8. Graphs of the measured crater volumes for a) Al_2O_3-based sample, c) Cr_2O_3-based samples and the changes in normalized crater volume for b) Al_2O_3-based samples d) Cr_2O_3-based samples. Constant excitation time, variable repetitions.

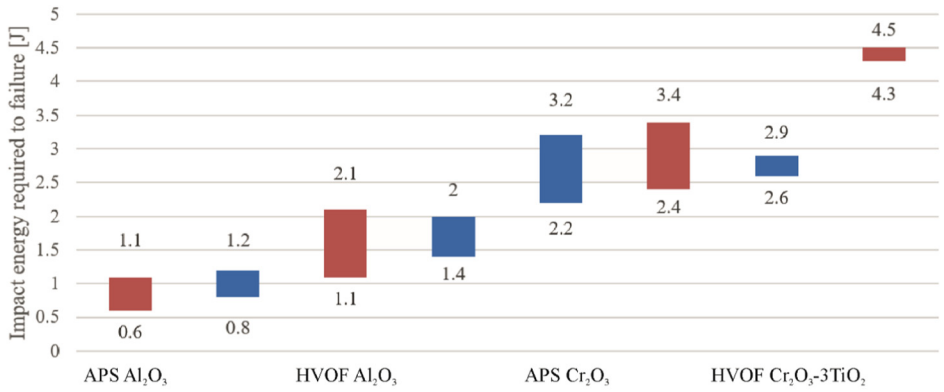

	HVOF Cr_2O_3		HVOF Cr_2O_3-5TiO_2		APS Al_2O_3-40ZrO_2		HVOF Al_2O_3-40ZrO_2	
Excit. Time (ms)	1	0.9	1.1	1.1	1.1	1	1	1.1
Repetititons	200	400	400	400	600	800	800	1000

Fig. 9. The cumulative impact energies required for failure in the second experimental set. Red bars indicate Al_2O_3-based samples and blue Cr_2O_3-based samples. In the table the excitation time and repetitions to failure are given. (For interpretation of the references to colour in this figure legend, the reader is referred to the web version of this article.)

experiment, highlighting the new information obtainable from the experiment.

4. Conclusion

The characteristics of micro-impact fatigue on thermally sprayed ceramic coatings were outlined in this study. Plasma- and HVOF-sprayed Al_2O_3, Al_2O_3-40ZrO_2 and Cr_2O_3 coatings and HVOF-sprayed Cr_2O_3-3TiO_2 and Cr_2O_3-5TiO_2 coatings were examined through an in-house made impact tester, where a 2 mm ZrO_2 sphere was fatiguing the coating surface with a frequency of 10 Hz and impact energies of 1.1–5.2 mJ. Two experimental set-ups were used. First, 1000 impacts were inflicted with varying energies. Second, based on the failure limit of the coating the impact energy was kept constant while the impact number was varied. The resulting impact craters were examined by optical microscopy and optical profilometry to determine the volume losses.

For all Al_2O_3-based coatings, aside from APS Al_2O_3-40ZrO_2, a cone crack was visible even with the lowest impact energies and it propagated quite gradually with increasing impact energies. The Cr_2O_3-based coatings were quite resistant to cone cracking but in the HVOF-sprayed samples the propagation was rapid and radial cracking leading to catastrophic failure appeared rapidly and clearly. Coinciding with this point of failure it was noticed that the normalized volume increment of the craters was 15 percentage points or more, an arbitrary number that gave good agreement with all coatings. This number is specific for the experiment, but the implication is that by following the evolution of damage in a ceramic coating an outlier in the trend can indicate that a limit of damage tolerance has been reached.

The coating material was deemed to be of little significance to the endurance of the coating. Rather, microstructural integrity and the residual stress state were extremely important, as evidenced by the positive effect of alloying of the base material in order to bring the composite melting temperature lower and to add a second phase to

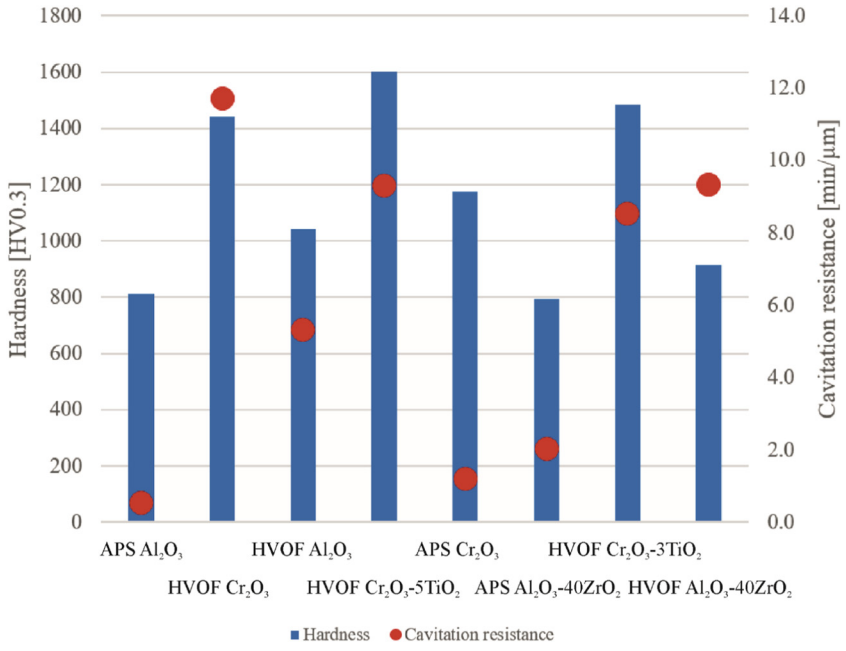

Fig. 10. Cavitation resistance and hardness of the coatings.

disperse the energy of cracking. Resistance to micro-impact fatigue was found not to correlate neither with coating microhardness nor cavitation erosion resistance, both of which are typically good indicators of structural cohesion and integrity. Therefore, the test gives a new approach into the research of the impact properties and fatigue life of thermally sprayed ceramic coatings. Further studies should focus on the relationship between micro-impact fatigue resistance and the thermal history and residual stress state of the coatings.

Acknowledgements

This work was supported by the graduate school of the President of Tampere University of Technology; and Business Finland (Finnish innovation funding, trade, investment, and travel promotion organization), its “Ductile & Damage Tolerant Ceramic Coatings”-project and the participating companies. The authors are grateful to Mr. Mikko Kylmälahti from Tampere University of Technology and Mr. Veli-Pekka Tarkiainen from Valmet Technologies Inc. (Jyväskylä, Finland) for spraying the coatings.

References

[1] P. Vuoristo, Thermal spray coating processes, in: S. Hashmi (Ed.), Compr. Mater. Process. Film. Coatings Technol. Recent Dev. Vol. 4 Elsevier, 2014, pp. 229–276, , https://doi.org/10.1016/B978-0-08-096532-1.00407-6.

[2] L. Pawlowski, The Science and Engineering of Thermal Spray Coatings, Second Ed, John Wiley & Sons, West Sussex, England, 2008, https://doi.org/10.1002/9780470754085.

[3] G. Bolelli, V. Cannillo, L. Lusvarghi, T. Manfredini, Wear behaviour of thermally sprayed ceramic oxide coatings, Wear 261 (2006) 1298–1315, https://doi.org/10.1016/j.wear.2006.03.023.

[4] E. Turunen, A. Hirvonen, T. Varis, T. Fält, S.-P. Hannula, T. Sekino, K. Niihara, Application of HVOF techniques for spraying of ceramic coatings, AZo J. Mater. Online. 3 (2007) 1–8, https://doi.org/10.2240/azojomo0260.

[5] E. Turunen, T. Varis, J. Keskinen, T. Fält, S.P. Hannula, Improved mechanical properties by nanoreinforced ceramic composite HVOF coatings, Adv. Sci. Tech. 45 (2006) 1240–1245, https://doi.org/10.4028/www.scientific.net/AST.45.1240.

[6] S.P. Hannula, E. Turunen, J. Keskinen, T. Varis, T. Fält, T.E. Gustafsson, R. Nowak, Development of nanostructured Al_2O_3-Ni HVOF coatings, Key Eng. Mater. 317–318 (2006) 539–544.

[7] D. Chen, E.H. Jordan, M. Gell, X. Ma, Dense TiO_2 coating using the solution precursor plasma spray process, J. Am. Ceram. Soc. 91 (2008) 865–872, https://doi.org/10.1111/j.1551-2916.2007.02225.x.

[8] J.W. Murray, A. Leva, S. Joshi, T. Hussain, Microstructure and wear behaviour of powder and suspension hybrid Al_2O_3–YSZ coatings, Ceram. Int. 44 (2018) 8498–8504, https://doi.org/10.1016/j.ceramint.2018.02.048.

[9] F.-L. Toma, L.-M. Berger, T. Naumann, S. Langner, Microstructures of nanostructured ceramic coatings obtained by suspension thermal spraying, Surf. Coat. Technol. 202 (2008) 4343–4348, https://doi.org/10.1016/j.surfcoat.2008.04.007.

[10] G. Bolelli, V. Cannillo, R. Gadow, A. Killinger, L. Lusvarghi, J. Rauch, Properties of high velocity suspension flame sprayed (HVSFS) TiO_2 coatings, Surf. Coat. Technol. 203 (2009) 1722–1732, https://doi.org/10.1016/j.surfcoat.2009.01.006.

[11] M.W. Barsoum, Fundamentals of Ceramics, 2nd ed., IOP Publishing, London, 2002.

[12] B.R. Lawn, Fracture and deformation in brittle solids: a perspective on the issue of scale, J. Mater. Res. 19 (2004) 22–29, https://doi.org/10.1557/jmr.2004.19.1.22.

[13] A. Evans, Perspective on the development of high-toughness ceramics, J. Am. Ceram. Soc. 73 (1990) 187–206, https://doi.org/10.1111/j.1151-2916.1990.tb06493.x.

[14] B. Lawn, R. Wilshaw, Indentation fracture: principles and applications, J. Mater. Sci. 10 (1975) 1049–1081, https://doi.org/10.1007/BF00823224.

[15] S.K. Lee, S. Wuttiphan, B.R. Lawn, Role of microstructure in Hertzian contact damage in silicon nitride, J. Am. Ceram. Soc. 80 (1997) 2367–2381, https://doi.org/10.1111/j.1151-2916.1997.tb03129.x.

[16] D.K. Kim, Y.G. Jung, I.M. Peterson, B.R. Lawn, Cyclic fatigue of intrinsically brittle ceramics in contact with spheres, Acta Mater. 47 (1999) 4711–4725, https://doi.org/10.1016/S1359-6454(99)00246-3.

[17] L. Ceseracciu, M. Anglada, E. Jiménez-Piqué, Influence of the elastic mismatch on the Hertzian cone crack path in ceramic bilayers, J. Eur. Ceram. Soc. 31 (2011) 1951–1955, https://doi.org/10.1016/j.jeurceramsoc.2011.04.032.

[18] J.B. Quinn, G.D.G. Quinn, Indentation brittleness of ceramics: a fresh approach, J. Mater. Sci. 2 (1997) 4331–4346, https://doi.org/10.1023/A:1018671823059.

[19] J. Kiilakoski, M. Lindroos, M. Apostol, H. Koivuluoto, V.-T. Kuokkala, P. Vuoristo, Characterization of high-velocity single particle impacts on plasma-sprayed ceramic coatings, J. Therm. Spray Technol. 25 (2016) 1127–1137, https://doi.org/10.1007/s11666-016-0428-2.

[20] R. Ahmed, M. Hadfield, Mechanisms of fatigue failure in thermal spray coatings, J. Therm. Spray Technol. 11 (2002) 333–349, https://doi.org/10.1361/105996302770348727.

[21] A. Vackel, S. Sampath, Fatigue behavior of thermal sprayed WC-CoCr-steel systems: role of process and deposition parameters, Surf. Coat. Technol. 315 (2017) 408–416, https://doi.org/10.1016/j.surfcoat.2017.02.062.

[22] A. Ibrahim, R.S. Lima, C.C. Berndt, B.R. Marple, Fatigue and mechanical properties of nanostructured and conventional titania (TiO_2) thermal spray coatings, Surf. Coat. Technol. 201 (2007) 7589–7596, https://doi.org/10.1016/j.surfcoat.2007.02.025.

[23] B.R. Lawn, Indentation of ceramics with spheres: a century after Hertz, J. Am. Ceram. Soc. 81 (2005) 1977–1994, https://doi.org/10.1111/j.1151-2916.1998.tb02580.x.

[24] R. Musalek, J. Matejicek, M. Vilemova, O. Kovarik, Non-linear mechanical behavior of plasma sprayed alumina under mechanical and thermal loading, J. Therm. Spray Technol. 19 (2010) 422–428, https://doi.org/10.1007/s11666-009-9362-x.

[25] J.H. Kim, S. Lee, K.S. Lee, D.K. Kim, The effect of grain boundary phase on contact damage resistance of alumina ceramics, J. Mater. Sci. 39 (2004) 7023–7030, https://doi.org/10.1023/B:JMSC.0000047547.09325.3d.

[26] A.C. Sekkal, C. Langlade, A.B. Vannes, A micro/macro impact test at controlled energy for erosion and phase-transformation simulation, Tribol. Lett. 15 (2003) 263–274, https://doi.org/10.1023/A:1024996621189.

[27] A.C. Sekkal, C. Langlade, A.B. Vannes, Tribologically transformed structure of titanium alloy ($TiAl_6V_4$) in surface fatigue induced by repeated impacts, Mater. Sci. Eng. A 393 (2005) 140–146, https://doi.org/10.1016/j.msea.2004.10.008.

[28] F. Ledrappier, C. Langlade, Y. Gachon, B. Vannes, Blistering and spalling of thin hard coatings submitted to repeated impacts, Surf. Coat. Technol. 202 (2008) 1789–1796, https://doi.org/10.1016/j.surfcoat.2007.07.107.

[29] G. Kermouche, C. Langlade, Mechanical nano-structuration of a C45 steel under repeated normal impacts, IOP Conf. Ser. Mater. Sci. Eng. 63 (2014) 012019, , https://doi.org/10.1088/1757-899X/63/1/012019.

[30] S. Kuroda, T.W. Clyne, The quenching stress in thermally sprayed coatings, Thin Solid Films 200 (1991) 49–66, https://doi.org/10.1016/0040-6090(91)90029-W.

[31] R.T.R. McGrann, D.J. Greving, J.R. Shadley, E.F. Rybicki, B.E. Bodger, D.A. Somerville, The effect of residual stress in HVOF tungsten carbide coatings on the fatigue life in bending of thermal spray coated aluminum, J. Therm. Spray Technol. 7 (1998) 546–552, https://doi.org/10.1361/105996398770350774.

[32] T. Varis, J. Knuuttila, T. Suhonen, U. Kanerva, J. Silvonen, J. Leivo, E. Turunen, Improving the properties of HVOF-sprayed Cr_2O_3 by nanocomposite powders, in: E. Lugscheider (Ed.), ITSC 2008 - Therm. Spray Crossing Borders, DVS-Verlag GmbH, Düsseldorf, Germany, Maastricht, the Netherlands, 2008, pp. 452–455.

[33] J. Kiilakoski, F. Lukac, H. Koivuluoto, P. Vuoristo, Cavitation wear characteristics of Al_2O_3-ZrO_2-ceramic coatings deposited by APS and HVOF processes, Proc. ITSC 2017, DVS Media GmbH, Düsseldorf, Germany, Düsseldorf, Germany, 2017, pp. 928–933.

[34] A. Kulkarni, J. Gutleber, S. Sampath, A. Goland, W.B. Lindquist, H. Herman, a.J. Allen, B. Dowd, Studies of the microstructure and properties of dense ceramic coatings produced by high-velocity oxygen-fuel combustion spraying, Mater. Sci. Eng. A 369 (2004) 124–137, https://doi.org/10.1016/j.msea.2003.10.295.

[35] R.S. Lima, B.R. Marple, Enhanced ductility in thermally sprayed titania coating synthesized using a nanostructured feedstock, Mater. Sci. Eng. A 395 (2005) 269–280, https://doi.org/10.1016/j.msea.2004.12.039.

[36] Y. Xie, H.M. Hawthorne, The damage mechanisms of several plasma-sprayed ceramic coatings in controlled scratching, Wear 233–235 (1999) 293–305, https://doi.org/10.1016/S0043-1648(99)00211-2.